# Dynamics of VOCs degradation and bacterial inactivation at the interface of AgxO/Ag/TiO2 prepared by HiPIMS under indoor light

M. Abidi, W. Abou Saoud, A. Bouzaza, A. Hajjaji, B. Bessais, D. Wolbert, Aymen Amin Assadi, S. Rtimi

# Dynamics of VOCs degradation and bacterial inactivation at the interface of $Ag_xO/Ag/TiO_2$ prepared by HiPIMS under indoor light

M. Abidi[1, 2,3], W. Abou Saoud[1], A. Bouzaza[1], A. Hajjaji[2], B. Bessais[2], D. Wolbert[1], A.A. Assadi[1]*, S. Rtimi[4]*

[1] Univ Rennes, Ecole Nationale Supérieure de Chimie de Rennes, CNRS, ISCR (Institut des Sciences Chimiques de Rennes) – UMR 6226, F-35000 Rennes, France
[2] Laboratoire de Photovoltaïque, Centre de Recherches et des Technologies de l'Energie, Technopole de Borj-Cédria, BP 95, 2050 Hammam-Lif, Tunisia
[3]Universite de Tunis El Manar, BP 94, Rommana, 1068 Tunis, Tunisia
[4] Ecole Polytechnique Fédérale de Lausanne, 1015 Lausanne, Switzerland

*** Corresponding authors:**

E-mail addresses: Aymen.assadi@ensc-rennes.fr (A. Assadi) and Rtimi.sami@gmail.com (S. Rtimi).

## Abstract

$Ag_xO/Ag/TiO_2$ photoactive thin films were produced by different modes of magnetron sputtering (namely, DCMS and HiPIMS). The spectral and microstructural properties of the Ag-$Ag_xO/TiO_2$ thin films were studied by Diffuse Reflection Spectroscopy (DRS) and X-Ray Photoemission Spectroscopy (XPS). The atomic deposition of TiO2 and Ag in the thin sputtered film were studied by TEM. $Ag_xO/Ag/TiO_2$ exhibited fast photocatalytic volatile organic compounds (VOCs) degradation and bacterial inactivation under low visible light intensity. The Langmuir Hinshelwood model was applied to highlight the photocatalytic performance of the $Ag_xO/Ag/TiO_2$ catalyst. The oxidative states of Ag-$Ag_xO/TiO_2$ were studied by XPS. Deconvolution of the Ag3d peak of the $Ag_xO/Ag/TiO_2$ thin films showed the presence of AgO and metallic Ag. It is suggested that the mechanism involving the degradation of VOCs on $AgO/Ag/TiO_2$ catalysts is due to the transfer of holes from AgO to $TiO_2$ via the $AgO/Ag/TiO_2$ heterojunction. The electrostatic interaction between both semiconductors allows this charge transfer. In addition, the contribution of reactive oxygen species (ROS) in bacterial inactivation at the interface of $AgO/Ag/TiO_2$ thin film was also examined. Light-induced interfacial charge transfer (IFCT) between AgO and $TiO_2$ leading to pollutants oxidation appears to require low photons' energy and can oxidize pollutants even at high concentrations. The sputtered coatings have also been studied for repetitive reuse, showing the sustainable activity of the prepared materials.

## Keywords

HiPIMS coating; Photocatalysis; indoor air treatment; Redox catalysis; Bacterial inactivation.

## 1. Introduction:

As it is largely connected to human health, indoor air quality has become a very important topic for the social, economic, and scientific community. It has been shown that modern society spends between 70% and 90% of their time indoors [1], such as

home, offices, cars, hospitals, and healthcare buildings… Besides, the world health organization declared that in 2012, 7 million premature deaths are due to air pollution. Amongst these 7 million deaths, 4.3 million were related to indoor contamination [2]. This is a complex problem containing different types of pollutants, such as particles (dust, and smoke…), radon, asbestos, biological agents (bacteria, viruses…), and gaseous contaminants such as ammonia [3-11]. Different sources are emitting VOCs such as outside pollution (food industry, swimming pool water treatment, hospital cleaning room….) and from everyday activities (e.g., cooking, smoking, or even using cleaning agents, and office equipment) [12-20]. To reduce the VOCs from air, various techniques were used, such as adsorption [21], condensation [22], plasma combined with catalysis [5-7,23-25], and photocatalysis [20,24]. Notwithstanding their significant ability in the VOCs removal, these proposed techniques were shown to produce high amounts of dangerous intermediates, by-products, and waste. Furthermore, these processes exhibit a temporary pollution transfer from gaseous to solid phase or pollution allocation from one area to another [27].

Heterogeneous photocatalysis is deemed as a promising method for air purification owing to its ability to remove VOCs even at relatively elevated concentrations [5, 7, 28-30]. This technique was able to degrade a wide range of pollutants and their by-products [31-33]. Titanium dioxide ($TiO_2$) is widely employed photocatalyst for pollutants' removal/abatement due to its high stability, excellent activity, inexpensive to build and operate, and its non-toxicity [40, 41]. $TiO_2$ supported on glass fiber tissue [34, 35], cellulosic paper [36], polymer support [34], and $TiO_2$ on PES fabrics [20, 37]. However, the main limiting factor affecting the photocatalytic application of $TiO_2$ in real settings is its wide band gap (3.2 eV) allowing only the absorption of UV photons [38, 39]. To extend the spectral absorption of $TiO_2$ in the visible light range, ionic (cationic or anionic) doping was seen to tighten its band gap allowing solar/visible light absorption [42-45] Other researchers adopted the engineering of tailored heterojunctions with other metal oxides allowing visible light absorption [39, 46-49].

In this study, we chose to combine $TiO_2$ with AgO to enhance the photocatalytic activity in the visible spectral range. $Ag_xO$ was chosen due to its strong plasmon resonance occurring under visible light excitation. The choice of $Ag_xO$ is favorable for energy levels' alignments that authorize the silver plasmonic electrons to be

transferred into the $TiO_2$. Both oxides were sputtered on textile fabrics to overcome the labor and time required to recover the catalyst after use.

This work addresses the synthesis of $Ag_xO$-$TiO_2$ on polyester cloth by two sputtering modes (DCMS and HiPIMS). Odorous compounds such as chloroform (Trichloromethane, $CHCl_3$) and Diacetyl (butane-2,3-dione, $(CH_3CO)_2$) were chosen as indoor VOCs models. Chloroforms are model pollutants commonly encountered in hospital settings. Diacetyl is normally emitted during food processing and preparation; they are dangerous to health [20]. In addition, the *E. coli* bacteria was chosen as a microorganism model. The effect of the applied sputtering mode on the kinetics of COVs removal (chloroform and butadione) and bacterial inactivation was studied and is presented in details in this work. The surface properties of the sputtered samples were examined by up-to-date surface science techniques. The prepared films will open the doors to potential applications in hospital settings to reduce bacterial infections and to remove malodors.

## 2. Experimental

### 2.1. Catalyst synthesis: Ag/$TiO_2$ sputtered PES

Ag and Ti were sputtered on PES using magnetron sputtering in the (HiPIMS and DCMS modes). The HiPIMS deposition was assisted with using a HiP3 5 kW Solvix generator at a time-average power of 100 W (5 $Wcm^{-2}$, pulse-width of 50 µs and a frequency of 1 kHz, gas phase 95% Ar - 5% $O_2$. The applied power to the Ti-target was 90 W for the first 30 s then at 50 W to regulate the relative content of Ti in the film as it will be shown later by transmission electron microscopy (TEM). The distance between the sputtered target and the sample holder was 10 cm as previously optimized [58]. The visual perception of the sputtered PES fabrics is shown in Figure 1.

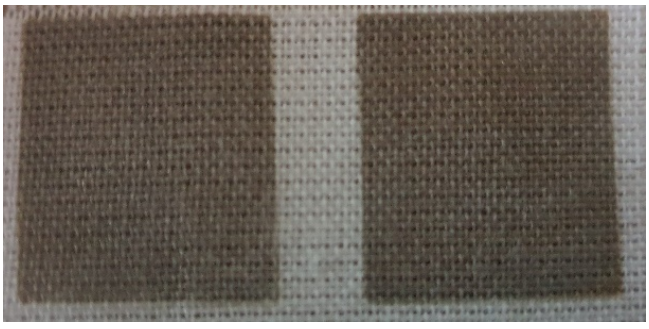

**Figure 1.** Visual perception of the $Ag_xO$-$TiO_2$ sputtered on PES.

### 2.2. Thickness of the sputtered AgxO-$TiO_2$-PES, TEM, spectral absorption and XPS

The thicknesses of $TiO_2$, Ag, and AgO-$TiO_2$ deposited on Si-wafer we measured using a Profilometer (Alphastep-500, Tencor, USA). To carry out TEM observations, the PES cloths were embedded in epoxy resin (Embd 812) and cross-sectioned with an ultra-microtome (Ultratcut E) and then imaged using FEI Osiris operated in 200kV. With Spot size of 5, dwell time 50 µs, real time 600 s.

Diffuse reflectance spectroscopy (DRS) was carried out by means of a Perkin Elmer Lambda 900 UV-VIS-NIR spectrometer within 250-700 nm wavelength range.

In order to determine the existing species on the sputtered $Ag_xO$-$TiO_2$ film, X-ray photoelectron spectroscopy (XPS) was performed using an AXIS NOVA photoelectron spectrometer (Kratos Analytical, Manchester, UK, monochromatic Al-$K_\alpha$ with $h\nu$ =1486.6 eV). In order to correct the charging effect at the interface of the sputtered samples, the carbon C1s line having position at 284.6 eV was used as reference. The surface atomic concentration was determined from the peak areas considering the sensitivity factors for each element. The XPS spectral peaks were deconvoluted using the CasaXPS V2 software.

### 2.3. Target compounds and tested bacteria

Two target organic compounds were used, Butadione ($C_4H_6O_2$) and Chloroform ($CHCl_3$), existing particularly in the food and hospital sectors, respectively. Butadione (99% purity) and Chloroform (99.4% purity) were used as VOCs probes. *Escherichia coli* (DSM 10198-0307-001) was used as a model microorganism to test the antibacterial activity. The preparation protocol and the testing method have been detailed before [20].

### 2.4. Reactor design for VOC removal

The used batch reactor has approximately 10 mm as upper diameter and 50 mm of working height contains two septa that are able to contain up to 50 mL of solution. The first one is used for samples extraction and the second one is used for VOCs injection. The catalytic samples were fixed to the internal wall of the batch reactor to be in direct contact with the studied VOC and light radiation. For all experiments, 20 $cm^2$ of coated $Ag_xO$-$TiO_2$-PES were used. A fluorescent visible lamp (Sylvania CF-L 24 W/840) with emission in the visible (400 – 720 nm) has been inserted inside the reactor. This light is a typical indoor light like those used for houses, hospitals and schools. To prevent extra-light from, the hall reactor was covered with Al-foil during the

photocatalytic experiments. The homogenization of the gas phase was allowed by a magnetic stirrer and barrel.

### 2.5. VOCs analysis system and antibacterial testing

To examine the performance of our catalysts for VOCs removal $C_4H_6O_2$ and $CHCl_3$ analysis was carried out using gas chromatography (Fisons GC9000) equipped with a FID. The mobile phase (carrier gas) was Nitrogen. We used a syringe of 500 µL for all injection. All injections were carried out in triplicates. Once the flow inside the reactor gets stabilized (at equilibrium), the pollutants analysis starts.

The antibacterial activity of $Ag_xO$-$TiO_2$-PES, *Escherichia coli* (*E. coli)* was studied as reported in our previous study [20]. In this study, the initial bacterial concentration is~ 2.6 $10^6$ colony-forming unit per milliliter (CFU/mL).

## 3. Results and discussion

### 3.1. Thickness calibration and TEM of sputtered $Ag_xO$-$TiO_2$-PES

Figure 2a presents the high-angle annular dark field (HAADF) mapping of elements in the $Ag_xO$-$TiO_2$-PES samples sputtered by HiPIMS at 30 A. Figures 2b, 2c and 2d show the mapping of Ti-, Ag-, and O-element, respectively. The Ag-atoms distribution (red image) appears to be dense and uniform. This likewise provides evidence for the presence of different oxidation states of Ag-NPs (AgO) in the topmost layers. In addition, many kinds of research studied in a detailed way the properties of Ag-coated PES [64-68]. The EDX mapping of oxygen clearly shows (Fig. 2d) relatively large amounts of oxygen species (purple image). This is due to $TiO_2$ (EDX mapping of Ti is shown in figure 2b) and AgO nanoparticles, which exhibit a higher O-content compared to the content of oxygen species in the film bulk. In the context of a comparison between the samples sputtered by DCMS and those sputtered by HiPIMS, Rtimi et al reported that the distribution of oxygen species in the samples sputtered by DCMS shows more oxidized copper (in this case Ag) species in the bulk than the samples prepared by HiPIMS, while the latter has shown more oxidized copper species at the upper layers in contact with bacteria [69].

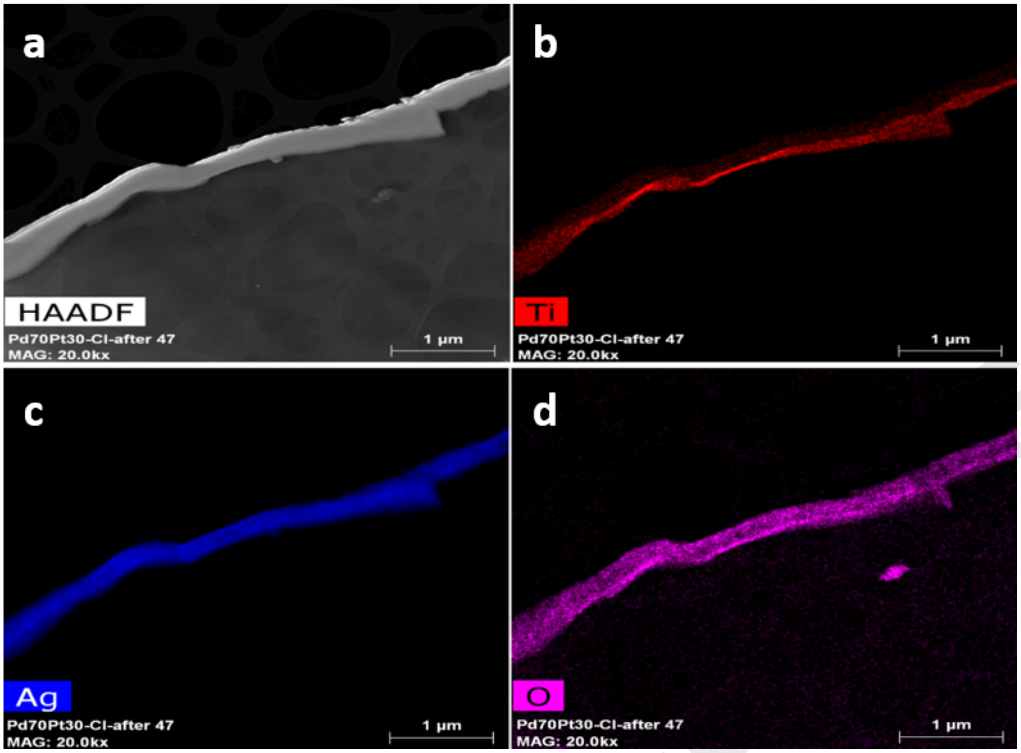


**Figure 2.** TEM images of $Ag_xO$-$TiO_2$-PES as sputtered by HiPIMS at a current of 30 A for 20s: a) High-angle annular dark-field imaging (HAADF), b) EDXS mapping of Ti, c) EDXS mapping of Ag, and d) EDXS mapping of O.

### 3.2. Surface properties of the sputtered $Ag_xO$-$TiO_2$-PES

Figure 3 shows the spectral absorption of the sputtered $Ag_xO$-$TiO_2$-PES by HiPIMS (at 30 A) and DCMS (at 0.3 A). Analysis of the absorption spectra show that $TiO_2$ thin film do not absorb in the visible and presented an absorption onset (λ) at 260 nm. In contrast, the light absorption of $Ag_xO/TiO_2$ sputtered by HiPIMS and DCMS extends to the visible region. In addition, a significant phenomenon was observed related to the interaction of light with The Ag incorporated into Titanium dioxide near the absorption edge. This was related to the interfacial charge transfer (IFCT) between AgxO and $TiO_2$ semiconductors [38]. A wide absorption band from 500 to 750 nm is noted for $AgxO/TiO_2$ photocatalysts sputtered by HiPIMS at 30A and DCMS at 0.3A. These bands can be ascribed to surface plasmon resonance (SPR) of the Ag species [38,44].

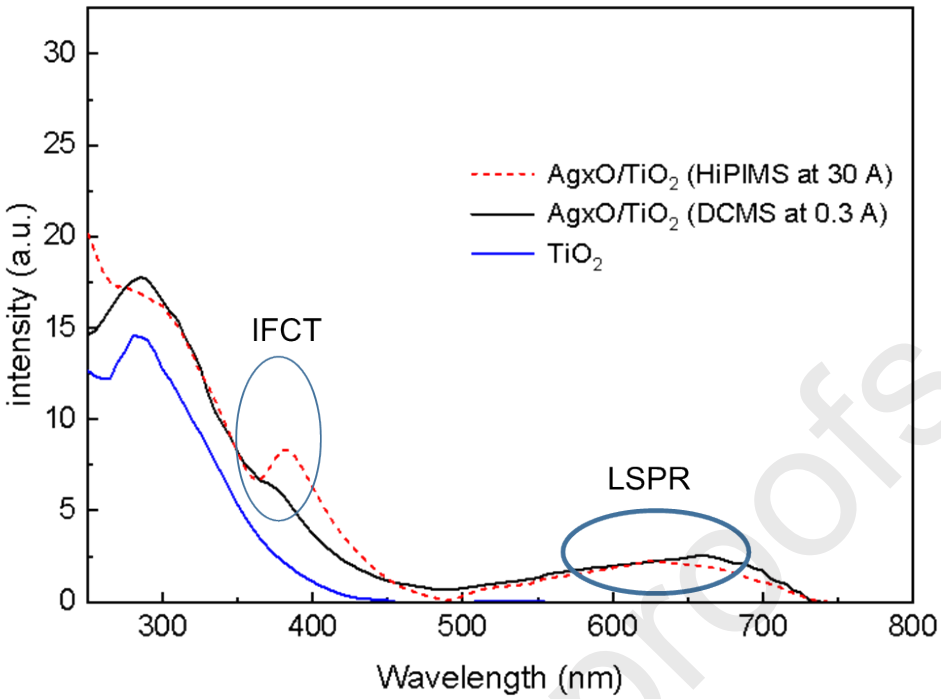


**Figure 3.** Diffuse reflectance spectroscopy (UV-Vis) of sputtered $TiO_2$ (using DCMS at 0.3 A) and $Ag_xO$-$TiO_2$ (using DCMS at 0.3 A and HiPIMS at 30 A).

In order to better analyze the light absorption of our coatings, we applied a spectral analysis based on high derivatives. The method of higher derivatives has been known for decades [70], but it has not previously been applied to the analysis of photocatalytic materials' spectra. Analysis of extrema in the representation of the second and fourth derivatives allows the determination of the UV-Vis absorption maxima giving a clear idea about the appropriate wavelengths to be used with this system. The signal-to-noise ratio in modern spectrometers is high enough to reliably determine higher derivatives. The fourth derivative of the absorption spectra allows to reliably determining the position of significant peaks. If these peaks overlap slightly, the second derivative becomes enough to locate the significant peaks. Figure 4 shows the second derivatives of the absorption spectra of (a) $TiO_2$ (using DCMS at 0.3 A) and $Ag_xO$-$TiO_2$ (using DCMS at 0.3A and HiPIMS at 30 A).

It is readily seen from the 2nd derivative of the Figure 4a ($AgxO/TiO_2$ (0.3 A)) that the thin film is absorbing at 350 nm and at 410 and 730 nm with a lower intensity. However, the thin $AgxO/TiO_2$ film prepared by HiPIMS exhibited higher spectral absorption peak at 350 nm than the film prepared by DCMS. In addition, the HiPIMS prepared film showed peaks at 420, 480 and 740 nm. The $TiO_2$ thin film showed only spectral

absorption in the UV range (320 and 365 nm). From Figure 4b, the HiPIMS thin film absorb in the UVA, violet and blue. This is attributed to the Ag surface plasmon. The weak peak at 730-740 nm refers to the far-red absorption.

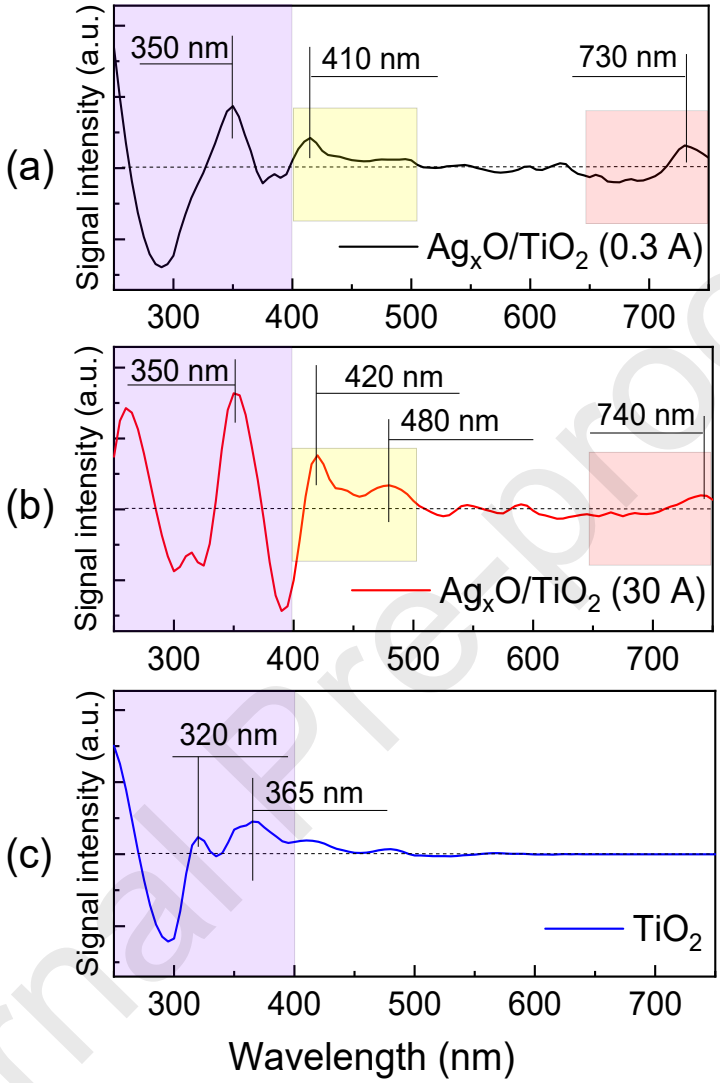


**Figure 4.** Analysis of spectral absorption extrema through second derivatives of light absorption of (a) AgxO/$TiO_2$ (0.3 A), (b) AgxO/$TiO_2$ (30 A) with respect to (c) sputtered $TiO_2$.

Figure 5 shows the oxidative states of Ag and Ti sputtered on the polyester cloth as determined by XPS. Figure 5 shows the Ti2p and Ag3d peaks from AgxO-$TiO_2$ deposited by HiPIMS and DCMS. The found peaks were asymmetric. AgO peaks at 367.6 eV were detected in both samples (HiPIMS and DCMS). The spectra showed also the presence of lower peaks at 368 eV characteristics of metallic Ag. The presence of Ti3+ in the HiPIMS samples could arise from the AgO incorporation on the $TiO_2$. The peak at 367.6 eV is characteristic of Ag-ions adsorbed on hydroxylated $TiO_2$ [71].

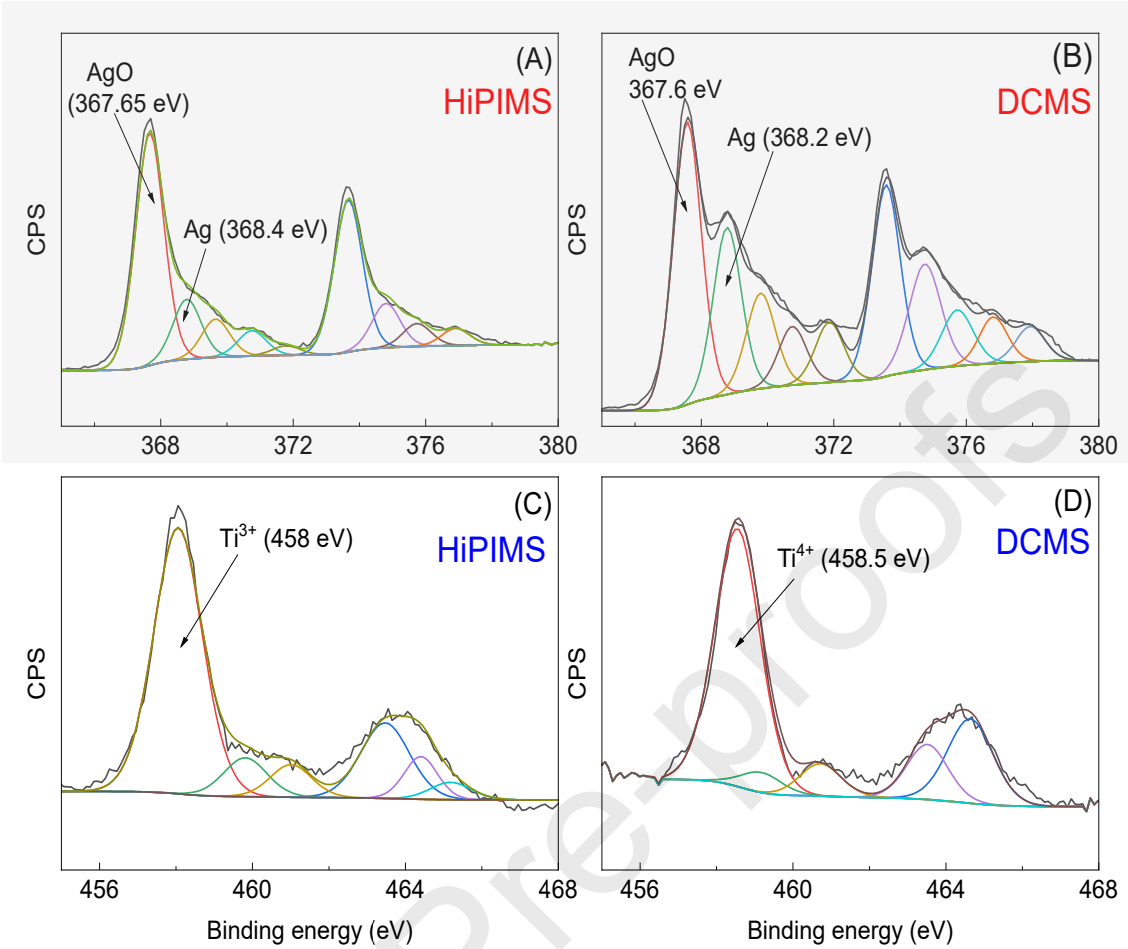


**Figure 5.** XPS deconvolution of Ag3d and Ti2p peaks from AgxO-$TiO_2$ deposited by HiPIMS and DCMS.

### 3.3. Photocatalytic experiments: COVs removal and Bacterial inactivation tests

#### *3.3.1. Effect of deposition of Ag-NPs $TiO_2$-PES by HiPIMS and DCMS on the photocatalytic activity of AgxO-$TiO_2$-PES photocatalyst*

The photocatalytic performances of AgxO-$TiO_2$-PES catalysts were evaluated by photocatalytic removal of COVs (Chloroform) under visible light irradiation at ambient temperature. Figure 6 shows the chloroform removal using AgxO-$TiO_2$-PES sputtered by HiPIMS for 10, 20, 30 A and sputtered by DCMS at 0.3A. Figure 6 shows that the chloroform removal is pertinently affected by the different sputtering current. In this test, it is readily seen that the initial concentrations of Chloroform decreased over time under visible light irradiation. Also, an increase in sputtering current from 10A until 30A increases the chloroform removal to about 98% of the initial concentration of 10 $g.m^{-3}$. This enhancement is due to the availability of active sites generated at the interface of the sample deposited at 30A [59]. However, at low current values the chloroform degradation reaches a limit; in fact, these current values are rather small to form a

catalyst layer leading to perfect and complete removal of chloroform. Previously S. Rtimi et al reported [69] that the HiPIMS deposition current generates different ions and charge species, leading to distinguish charges at the interfaces of the thin film. In addition, compared to the AgxO-$TiO_2$-PES sputtered by direct current magnetron sputtering (DCMS) at 0.3A, AgxO-$TiO_2$-PES (HiPIMS at 30A) exhibits a high photocatalytic activity under visible light. This is due to the generation of a higher number of Ag-ions at the catalysts surface when using HiPIMS (30A) than DCMS [64, 69].

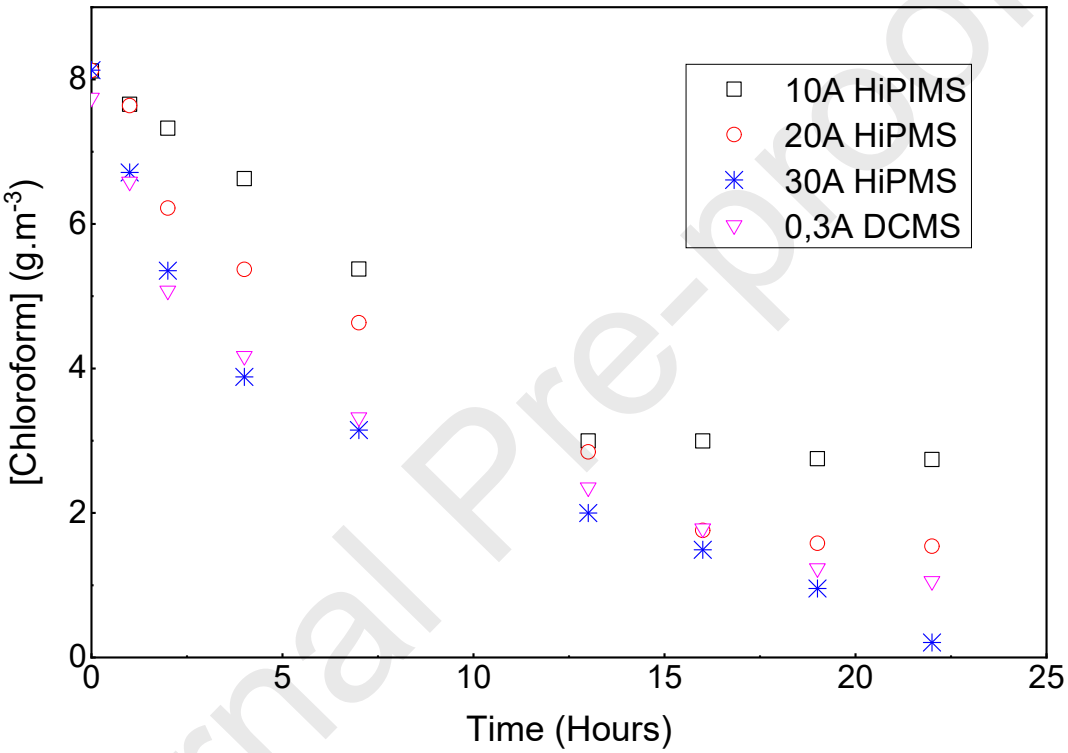


**Figure 6.** Removal of chloroform with catalyst AgxO-TiO2-PES at different HiPIMS sputtering currents deposited for 20 s. Light source: fluorescent visible lamp (Sylvania CF-L 24 W/840; 400 – 720 nm)

### *3.3.2. Mixtures of pollutants (VOCs and bacteria)*

#### *3.3.2.1. Effect of the presence of two Kinds of VOCs on AgxO-$TiO_2$-PES performance*

The removal performance of two kinds of indoor air pollutants, with equimolar concentrations, was investigated. Figure 7 shows that at 30A HiPIMS and low visible light illumination, the degradation of Chloroform is quite similar to that of Butadione

(BUT). Firstly, before switching on the lamp and during the adsorption stage, it was found that the adsorbed Butadione amount is slightly greater than that of chloroform. Once adsorption of both species reaches saturation, the lamp is switched on. We found (Fig. 7) that that the photocatalytic degradation kinetics of BUT is faster than that of chloroform. This may be attributed to the chemical composition of the pollutants (e.g., carbon number), their affinities to the catalyst and the amounts of their intermediate by-products on the catalyst surface, which in turn leads to a competitive effect of the pollutants towards the active catalytic sites. This result is similar to our previous work [20] where we used $Cu_xO/TiO_2$-PES for the removal of VOCs.

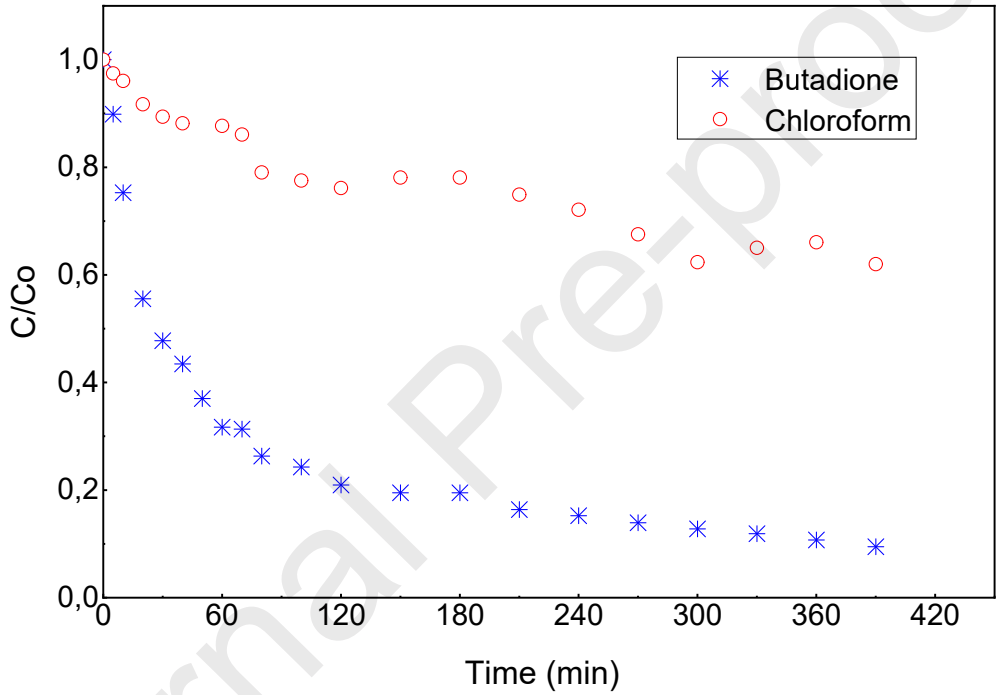


**Figure 7.** Two kinds of Indoor air pollutants removal on AgxO-$TiO_2$-PES HiPIMS-sputtered 30 A for 20 s under a fluorescent visible lamp (Sylvania CF-L 24 W/840; 400 – 720 nm)

Figure 8 shows the BUT degradation in the presence of the AgxO-$TiO_2$-PES photocatalyst under light starting with different initial concentrations. The degradation rate decreases when the BUT initial concentration increases. This is owing to the availability of active catalytic sites at low concentrations [58, 70]. Indeed, the amount of the molecules involved in the reaction is not increased in the same ratio than that of the inserted initial concentration resulting in a decrease in the degradation efficiency.

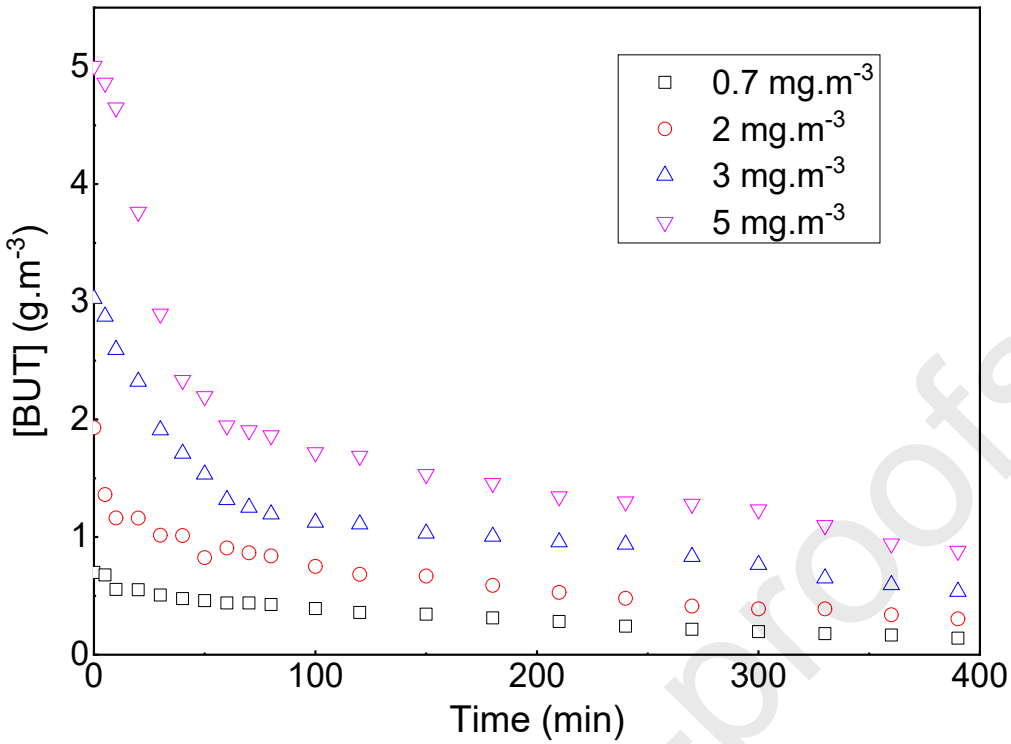


**Figure 8.** BUT degradation versus inlet BUT concentration under visible light irradiation (Sylvania CF-L 24 W/840; 400 – 720 nm) based on HiPIMS sputtered AgxO-$TiO_2$-PES (30 A for 20 s).

To further understand the chemical transformation of the heterogeneous photocatalytic degradation of Butadione over AgxO-$TiO_2$-PES, the Langmuir-Hinshelwood (L-H) model was employed to fit the experimental results [58, 71]. The L-H reaction rate equation shown in the following equation is employed to explain the adsorption and degradation of Butadione:

$$r_0 = -\frac{d[VOC]}{dt} = k_c \frac{K[VOC]_0}{1 + K[VOC]_0}$$

Where $r_0$ (mmol/$g_{cat}$ $m^3$ s) is the initial photocatalytic degradation rate, $[VOC]_0$ is the initial BUT concentration (mmol/$m^3$), $K$ is the adsorption constant ($m^3$/mmol) and $k_c$ is the kinetic constant (mmol.$m^{-3}$ s $g_{TiO2}$) at maximum coverage for the experimental conditions.

The plot of $1/r_0$ versus $1/[COV]_0$ enables determining the values of $k_c$ and $K$. According to Figure 9, we estimate the values of the kinetic and adsorption constants (Table 1) using the linearized L-H equation ( $\frac{1}{r_0} = \frac{1}{k_c K} \times \frac{1}{[VOC]_0} + \frac{1}{k_C}$ ).

Table 1 shows Butadione shows a slow degradation rate regarding the use of AgxO-$TiO_2$-PES sputtered at 30A; this may be due to the physicochemical properties of the pollutant and to the interfacial charge transfer mechanism (IFCT), which will be shown in a later section.

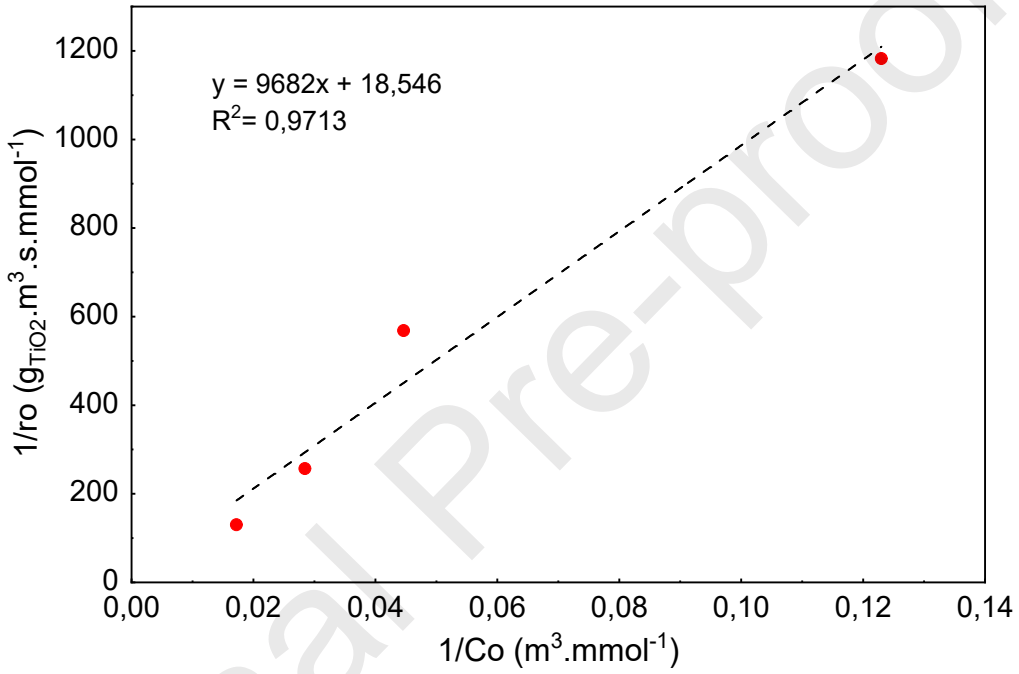


**Figure 9.** Linear regression using L-H model for the BUT degradation on AgxO-$TiO_2$-PES sputtered at 30A for 20s.

**Table 1.** L-H constants ($k_c$ and K) at AgxO-$TiO_2$-PES photocatalyst

| Catalyst tested | $k_c$: Kinetic constant of L-H (mmol.$m^{-3}$. s. $g_{TiO2}$) | K: Adsorption Constant of L-H ($m^3$. $mmol^{-1}$) |
|---|---|---|
| AgxO-$TiO_2$-PES | 54 $10^{-3}$ | 2 $10^{-3}$ |

Table 1 shows that AgxO-$TiO_2$-PES leads to a more efficient degradation of butadione compared to PES-$TiO_2$, which in turn leads to an almost twice faster degradation of butyraldehyde under UV irradiation [59]. This result may be due to the Ag amount

present on the photocatalyst surface and to the chemical properties of the target pollutants.

### *3.3.2.2. Simultaneous removal of butadione and bacteria*

After studying the effect of the existence of two kinds of indoor air pollutants on AgxO-$TiO_2$-PES performance, we investigate the bacterial (*E. coli*) inactivation activity of AgxO-$TiO_2$-PES together with simultaneous removal of BUT and *E. coli*. Many experiments were done with our composites with initial bacterial concentration and inlet BUT concentration of ~ 2.6 $10^6$ (CFU/mL) and 5 mg/$m^3$, respectively. In fact, the goal of mixing target molecules with bacteria is to validate the effectiveness of the advanced oxidation process (AOP) in a case closer to real conditions where large amounts of pollutants must be removed simultaneously, and to see that there is always a degradation of pollutants during mixing. Figure 10 shows the bacterial inactivation performance of AgxO-$TiO_2$-PES during separate and simultaneous removal of BUT and *E. coli* under visible light irradiation.

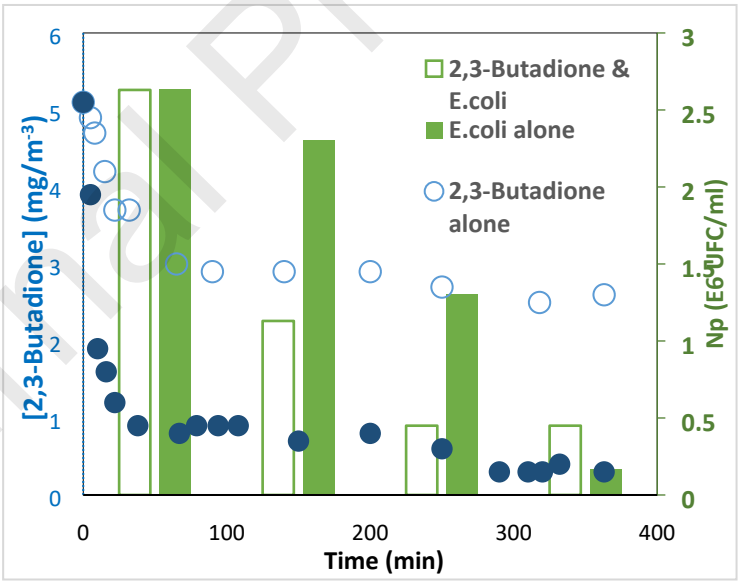


**Figure 10.** Simultaneous removal of *E. coli* and BUT on AgxO-$TiO_2$-PES catalyst sputtered at a peak current of 30A. The initial concentration of *E. coli* is ~2.6 $10^6$ CFU/mL. (Light source: Sylvania CF-L 24 W/840; 400 – 720 nm).

## 3.4. Identification of the VOCs' degradation by-products

The by-products emanating from the photocatalytic degradation of butadione in presence of bacteria using the AgxO-$TiO_2$-PES catalyst were determined by Gaseous Chromatography-Mass Spectroscopy (GC-MS). Figure 11 shows GC-MS spectra of

by-products originating from AgxO-$TiO_2$-PES – based Butadione photo degradation. The detected degradation by-products are: (i) acetone ($C_3H_5O$), (ii) acetaldehyde ($C_2H_4O$) and (iii) acetic acid ($C_2H_4O_2$). Butadione ($C_4H_6O_2$) is also present after 4.83 minutes. These results are similar to those reported by Abou Saoud et al. [5], subsequent to the use of $TiO_2$-GFT (Glass Fiber Tissue) as photo-catalyst for butadione degradation under photocatalytic/plasma processes.

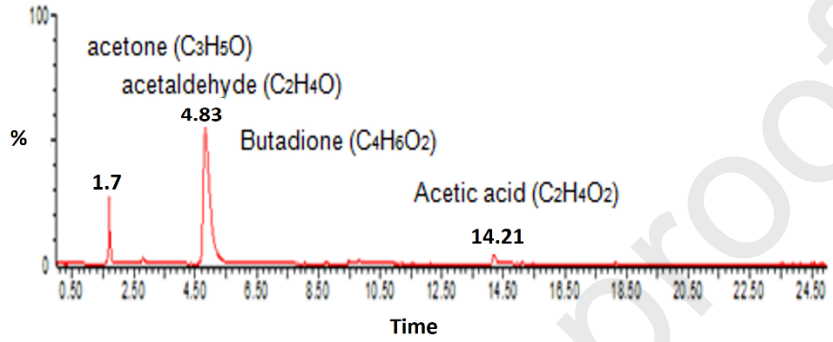


**Figure 11.** GC-MS of products observed during Butadione photo degradation by AgxO-$TiO_2$-PES.

### 3.5. Catalyst recyclability

The reusability of the catalyst is an important factor to take into account since it concerns the possibility of its potential application in environments polluted by toxic gases [20]. The re-use of the catalyst was examined for four successive cycles. The AgxO-$TiO_2$-PES was washed well after each photodegradation cycle and reused. Figure 12 shows no loss of sample photoactivity after four cycles of use. These results prove the overall potential of the AgxO-$TiO_2$-PES to be used as photocatalyst for air treatment applications. Furthermore, the same slope is noted in each cycle; these results can confirm the non-deactivation of the surface sites of the catalyst and its excellent catalytic stability.

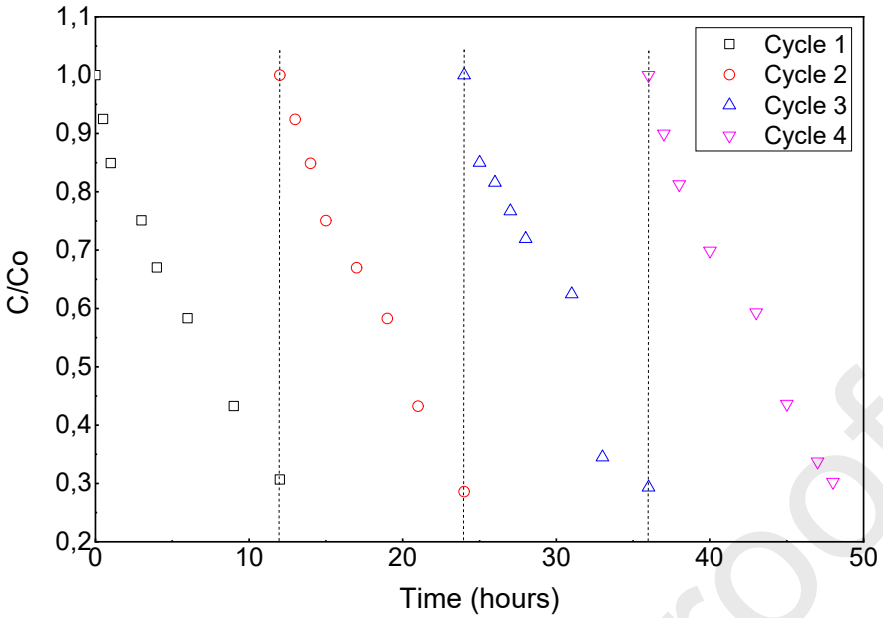


**Figure 12.** Repetitive degradation of Butadione on $Ag_xO$-$TiO_2$-PES. VOC concentration = 10g/$m^3$.

### 3.6. Photocatalytic degradation mechanism

To understand the possible photocatalytic mechanism of VOC removal and E. coli inactivation in $Ag_xO/TiO_2$ composite, Figure 13 was proposed. Under UV-vis light, electron-hole pairs generate in the valence bands (VB) of AgO and $TiO_2$, then migrate to the conduction bands (CB). The AgO conduction band potential was 0.72 eV and the Ag Fermi level was 0.99 eV [72]. As a result, and because the Fermi level of Ag was more positive than the conduction band potential of AgO, the electrons that are in the AgO conduction band can move to the Fermi level of Ag. At the same time, electrons on the Fermi level of Ag can be rapidly transferred to the $TiO_2$ semiconductor interface, which has been reported in Ag/ZnO and $Ag/TiO_2$ systems [73,74]. This could be due to the fact that the heterojunction in $Ag\text{-}AgO/TiO_2$ assisted the transfer of photo-generated electrons and holes. Thus, these electrons can quickly be transferred into the $TiO_2$ interface and then undergo a transformation as described below:

$$AgO/TiO_2 + h\upsilon \rightarrow e^- + h^+ \quad (1)$$

$$e^- + h^+/AgO \rightarrow e^-/Ag \rightarrow e^-/TiO_2 \quad (2)$$

$$O_2 + e^- \rightarrow O_2^{\bullet-} \quad (3)$$

$$O_2^{\bullet-} + 2H_2O + 2e^- \rightarrow 3OH^- + {}^{\bullet}OH \quad (4)$$

In reaction (4), one can describe it as a multi-electron transfer process. However, the activation energy of such reactions, as follows from the Marcus theory [75], is directly proportional to the square of the number of transferred electrons. The proposed mechanism is then described as the classical chain degenerated-branched oxidation of organic materials (eqs.5-11) [76-78]:

$h^+ + OH^- \rightarrow {}^{\bullet}OH$ (-1.9 eV) (5)

$h^+ + RH \rightarrow R^{\bullet} + H^+$ (6)

$O_2^- + H^+ \rightarrow HO_2^{\bullet}$ (7)

$HO_2^{\bullet} + RH \rightarrow HOOH + R^{\bullet}$ (8)

$R^{\bullet} + O_2 \rightarrow RO_2^{\bullet}$ (9)

$RO_2^{\bullet} + RH \rightarrow ROOH + R^{\bullet}$ (10)

HOOH, ROOH + e- [M (possible participation of the reduced metal ion)] $\rightarrow {}^{\bullet}OH, RO^{\bullet}$ + $HO\text{-}HO^{\bullet}, RO^{\bullet} + RH \rightarrow H_2O, ROH + R^{\bullet}$ (11)

Reaction can be simplified as seen in eq.12:

VOC/Bacteria + $O_2^{\bullet-}$ /${}^{\bullet}OH \rightarrow CO_2 + H_2O$ + dead bacteria + other products (12)

At the same time, the photo-generated holes in the Valence band of $TiO_2$ are easily transferred to the Valence band of AgO. This result could be due to the fact that the Valence band of AgO (1.84 eV) is more negative than that of $TiO_2$ (~3eV). Therefore, while the photo-generated electrons flow on the $TiO_2$ surfaces, the holes are gathered in the AgO Valence band. Therefore, it was constructed an inter-semiconductor transfer flows for electrons ($AgO \rightarrow Ag \rightarrow TiO_2$) and holes ($TiO_2 \rightarrow AgO$), which significantly limited the charge recombination and improved the charge separation efficiency. The fact that there was effective charge separation resulted in an increase in the lifetime of photogenerated charges, which increased the photocatalytic performance of our photocatalyst. Indeed, adsorbed oxygen ($O_2$) and water ($H_2O$) reacted with electrons ($e^-$) and holes ($h^+$) to produce the superoxide anion ($O_2^{\cdot-}$), hydroxyl radical ($OH^{\cdot}$), OH and $H^+$. The superoxide anion $0_2^{\cdot-}$ and the hydroxyl radical ($OH^{\cdot}$) were considered to be highly oxidizing reactive oxygen species (ROS). They can decompose VOCs, bacteria and other organic materials adsorbed on the active sites of the nanocomposites into $CO_2$, $H_2O$ and other products, as shown in eq. (1-12).

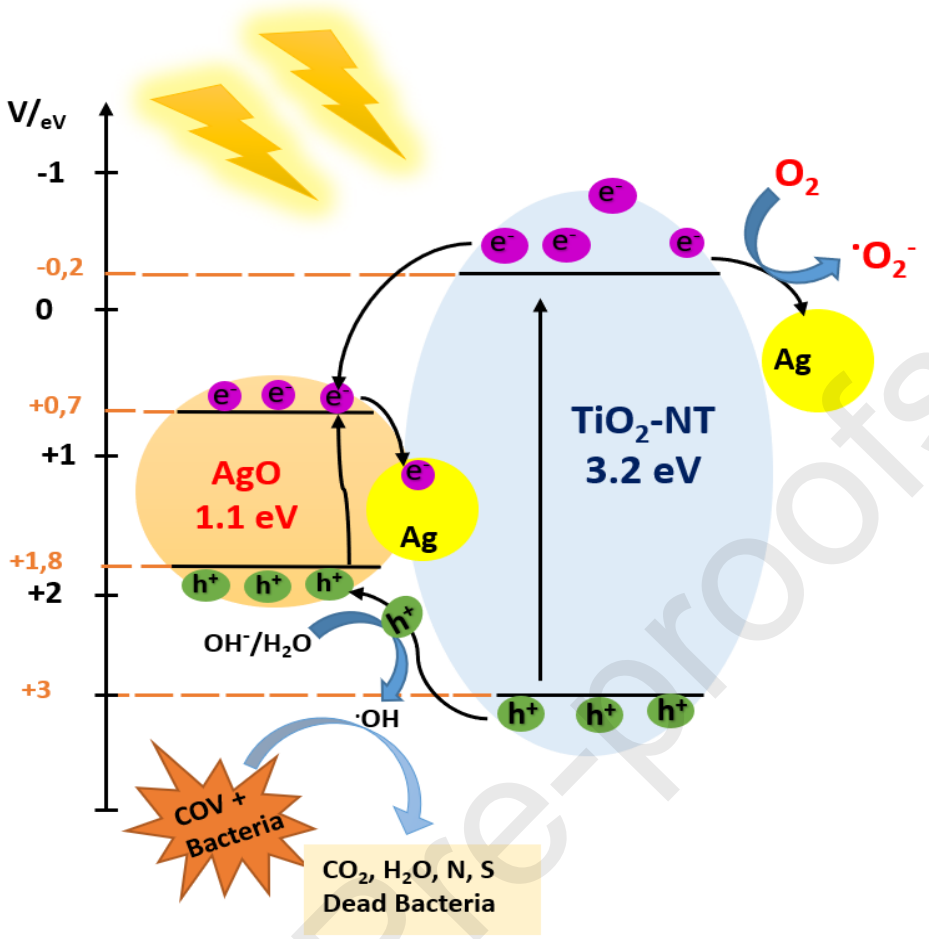


**Figure 13.** Proposed mechanism of photocatalysis by Ag-AgO/$TiO_2$ nanocomposite under light.

## 4. Conclusion

This paper reports the testing of a novel, uniform and stable AgxO/$TiO_2$-PES photocatalyst prepared at low temperature by high power pulsed magnetron sputtering. This is the first study where uniform Ag/AgxO coatings on PES were used for the degradation of indoor air VOCs as well as for bacterial deactivation. We have studied the degradation of two types of concentrated VOCs (butadione and chloroform) using the $Ag_xO/TiO_2$-PES catalyst. We have shown that this catalyst has stable performance during the removal of butadione by $Ag_xO/TiO_2$-PES. Likewise, this catalyst gives almost reproducible results and good recyclability when used under visible irradiation. It also exhibits excellent catalytic stability and has promising potential for application in air treatment. The $Ag_xO/TiO_2$-PES photocatalyst showed high antibacterial activity, which reached almost complete bacterial inactivation within 6 hours for $Ag_xO$ sputtered at 30 A.

**Acknowledgement:** SR would like to thank Profs. H. Hofmann and C. Pulgarin. This study was partly supported by NanoScreen CCMX Materials Challenge Project (EPFL-STI-IMXLTP).

## References

[1] A. Bacaloni, S. Insogna, L. Zoccolillo, Indoor Air Quality. Volatile Organic Compounds: Sources, Sampling and Analysis. In Chemistry, Emission Control, Radioactive Pollution and Indoor Air Quality. IntechOpen (2011).

[2] World Health Organization (WHO) (2014) Public health, environmental and social determinants of health (PHE), Geneva. https://www.who.int/phe/health_topics/outdoorair/databases

[3] B. Guieysse, C. Hort, V. Platel, R. Munoz, M. Ondarts, S. Revah, Biological treatment of indoor air for VOC removal: Potential and challenges. Biotechnology advances, 26 (2008), pp. 398-410.

[4] A. P. Jones, Indoor air quality and health. Atmospheric environment, 33 (1999), pp. 4535-4564.

[5] W. A. Saoud, A. A. Assadi, A. Kane, A. V. Jung, P. Le Cann, A. Gerard, F. Bazantay, A. Bouzaza, D. Wolbert, Integrated process for the removal of indoor VOCs from food industry manufacturing: Elimination of Butane-2, 3-dione and Heptan-2-one by cold plasma-photocatalysis combination. Journal of Photochemistry and Photobiology A: Chemistry, 386 (2020), p. 112071.

[6] W. A. Saoud, A. A. Assadi, M. Guiza, S. Loganathan, A. Bouzaza, W. Aboussaoud, A. Ouederni, S. Rtimi, D. Wolbert, Synergism between non-thermal plasma and photocatalysis: Implications in the post discharge of ozone at a pilot scale in a catalytic fixed-bed reactor. Applied Catalysis B: Environmental, 241 (2019), pp. 227-235.

[7] A. A. Assadi, A. Bouzaza, D. Wolbert, Study of synergetic effect by surface discharge plasma/$TiO_2$ combination for indoor air treatment: Sequential and continuous configurations at pilot scale. Journal of Photochemistry and Photobiology A: Chemistry, 310 (2015), pp. 148-154.

[8] EPA, U. (2017). Volatile Organic Compounds Impact on Indoor Air Quality. Recuperado de: https://www. EPA. Gov/indoor-air-quality-iaq/volatile-organiccompounds-impact-indoor-air-quality# intro.

[9] R. Montero-Montoya, R. López-Vargas, O. Arellano-Aguilar, Volatile organic compounds in air: sources, distribution, exposure and associated illnesses in children. Annals of global health, 84 (2018), pp. 225.

[10] J. Gu, Z. Wang, J. Kuen, L. Ma, A. Shahroudy, B. Shuai, T.Chen, Recent advances in convolutional neural networks. Pattern Recognition, 77 (2018), pp. 354-377.

[11] S. C. Lee, W. M. Li, , C. H. Ao, Investigation of indoor air quality at residential homes in Hong Kong—case study. Atmospheric Environment, 36 (2002), pp. 225-237.

[12] W. T. Tsai, An overview of health hazards of volatile organic compounds regulated as indoor air pollutants. Reviews on environmental health, 34 (2019), pp. 81-89.

[13] C. Lorimier, A. Subrenat, L. Le Coq, P. Le Cloirec, Adsorption of toluene onto activated carbon fibre cloths and felts: application to indoor air treatment. Environmental technology, 26 (2005), pp. 1217-1230.

[14] F. Squinazi, La pollution de l'air à l'intérieur des bâtiments (allergènes exclus). Revue française d'allergologie et d'immunologie clinique, 42 (2002), pp. 248-255.

[15] W. G. Tucker, Volatile organic compounds. Indoor air quality handbook, 31 (2001), pp. 1-20.

[16] C. C. Chan, J. D. Spengler, H. Özkaynak, M. Lefkopoulou, Commuter exposures to VOCs in Boston, Massachusetts. Journal of the Air & Waste Management Association, 41 (1991), pp. 1594-1600.

[17] N. J. Lawryk, C. P. Weisel, Concentrations of volatile organic compounds in the passenger compartments of automobiles. Environmental science & technology, 30 (1996), pp. 810-816.

[18] M. Dechow, H. Sohn, J. Steinhanses, Concentrations of selected contaminants in cabin air of airbus aircrafts. Chemosphere, 35 (1997), pp. 21-31.

[19] C.Y. Chao and G.Y. Chan, Quantification of indoor VOCs in twenty mechanically ventilated buildings in Hong-Kong, Atmos. Environ., 35 (2001), pp. 5895-5913.

[20] M. Abidi, A. A. Assadi, A. Bouzaza, A. Hajjaji, B. Bessais, S. Rtimi, Photocatalytic indoor/outdoor air treatment and bacterial inactivation on CuxO/$TiO_2$ prepared by HiPIMS on polyester cloth under low intensity visible light. Applied Catalysis B: Environmental, 259 (2019), p. 118074.

[21] J. Matos, A. Garcia, J. M. Chovelon, C. Ferronato, Combination of adsorption on activated carbon and oxidative photocatalysis on $TiO_2$ for gaseous toluene remediation. The Open Materials Science Journal, 4 (2010).

[22] M. Wang, A. Lawal, P. Stephenson, J. Sidders, C. Ramshaw, Post-combustion $CO_2$ capture with chemical absorption: a state-of-the-art review. Chemical engineering research and design, 89 (2011), pp. 1609-1624.

[23] A. A. Assadi, A. Bouzaza, I. Soutrel, P. Petit, K. Medimagh, D. Wolbert, A study of pollution removal in exhaust gases from animal quartering centers by combining photocatalysis with surface discharge plasma: from pilot to industrial scale. Chemical Engineering and Processing: Process Intensification, 111 (2017), pp. 1-6.

[24] A. A. Assadi, A. Bouzaza, C. Vallet, D. Wolbert, Use of DBD plasma, photocatalysis, and combined DBD plasma/photocatalysis in a continuous annular reactor for isovaleraldehyde elimination–synergetic effect and byproducts identification. Chemical Engineering Journal, 254 (2014), pp. 124-132.

[25] G. Maxime, A. A. Amine, B. Abdelkrim, W. Dominique, Removal of gas-phase ammonia and hydrogen sulfide using photocatalysis, nonthermal plasma, and

combined plasma and photocatalysis at pilot scale. Environmental Science and Pollution Research, 21 (2014), pp. 13127-13137.

[26] P. M. Huck, W. B. Anderson, S. M. Rowley, S. A. Daignault, Formation and removal of selected aldehydes in a biological drinking-water treatment process. Aqua (London), 39 (1990), pp. 321-333.

[27] A. A. Assadi, A. Bouzaza, D. Wolbert, P. Petit, Isovaleraldehyde elimination by UV/$TiO_2$ photocatalysis: comparative study of the process at different reactors configurations and scales. Environmental Science and Pollution Research, 21 (2014), pp. 11178-11188.

[28] V. Binas, D. Venieri, D. Kotzias, G. Kiriakidis, Modified $TiO_2$ based photocatalysts for improved air and health quality. Journal of Materiomics, 3 (2017), pp. 3-16.

[29] L. Zhong, F. Haghighat, Photocatalytic air cleaners and materials technologies–Abilities and limitations. Building and Environment, 91 (2015), pp. 191-203.

[30] W. A. Saoud, A. A. Assadi, M. Guiza, A. Bouzaza, W. Aboussaoud, A Ouederni, S. Rtimi, Study of synergetic effect, catalytic poisoning and regeneration using dielectric barrier discharge and photocatalysis in a continuous reactor: Abatement of pollutants in air mixture system. Applied Catalysis B: Environmental, 213 (2017), pp. 53-61.

[31] J. Mo, Y. Zhang, Q. Xu, J. J. Lamson, R. Zhao, Photocatalytic purification of volatile organic compounds in indoor air: a literature review. Atmospheric environment, 43 (2009), pp. 2229-2246.

[32] D. Farhanian, F. Haghighat, Photocatalytic oxidation air cleaner: identification and quantification of by-products. Building and environment, 72 (2014), pp. 34-43.

[33] M. Sleiman, P. Conchon, C. Ferronato, J. M. Chovelon, Photocatalytic oxidation of toluene at indoor air levels (ppbv): Towards a better assessment of conversion, reaction intermediates and mineralization. Applied Catalysis B: Environmental, 86 (2009), pp. 159-165.

[34] W. A. Saoud, A. A. Assadi, M. Guiza, A. Bouzaza, W. Aboussaoud, A. Ouederni, S. Rtimi, Study of synergetic effect, catalytic poisoning and regeneration using dielectric barrier discharge and photocatalysis in a continuous reactor: Abatement of pollutants in air mixture system. Applied Catalysis B: Environmental, 213 (2017), pp. 53-61.

[35] A. Y. Shan, T. I. M. Ghazi, S. A. Rashid, Immobilisation of titanium dioxide onto supporting materials in heterogeneous photocatalysis: a review. Applied Catalysis A: General, 389 (2010), pp. 1-8.

[36] A. A. Assadi, A.Bouzaza, D. Wolbert, Photocatalytic oxidation of trimethylamine and isovaleraldehyde in an annular reactor: Influence of the mass transfer and the relative humidity. Journal of Photochemistry and Photobiology A: Chemistry, 236 (2012), pp. 61-69.

[37] H. Zeghioud, N. Khellaf, A. Amrane, H. Djelal, W. Elfalleh, A. A. Assadi, S. Rtimi, Photocatalytic performance of $TiO_2$ impregnated polyester for the degradation of Reactive Green 12: Implications of the surface pretreatment and the

microstructure. Journal of Photochemistry and Photobiology A: Chemistry, 346 (2017), pp. 493-501.

[38] M. Ozimek, M. Palewicz, A. Hreniak,. Optical Properties of TiO 2 Nanopowder Doped by Silver (Copper) during Synthesis or PVD Method. *Acta Physica Polonica,* A., 129 (2016) (6).

[39] A. Hajjaji, M. Elabidi, K. Trabelsi, A. A. Assadi, B. Bessais, S. Rtimi, Bacterial adhesion and inactivation on Ag decorated $TiO_2$-nanotubes under visible light: Effect of the nanotubes geometry on the photocatalytic activity. Colloids and Surfaces B: Biointerfaces, 170 (2018), pp. 92-98.

[40] J. Das, E. R. Rene, J. Krishnan, Photocatalytic degradation of volatile pollutants. J Environ Chem Toxicol Vol, 2 (2018).

[41] K. W. Shah, W. Li, A Review on Catalytic Nanomaterials for Volatile Organic Compounds VOC Removal and Their Applications for Healthy Buildings. Nanomaterials, 9 (2019), p. 910.

[42] R. AP Ribeiro, S. R de Lazaro, C. R de Oliveira, Band-Gap engineering for photocatalytic applications: Anionic and cationic doping of $TiO_2$ anatase. Current Physical Chemistry, 6 (2016), 22-27.

[43] N. Delegan, R. Daghrir, P. Drogui, M. A. El Khakani, Bandgap tailoring of in-situ nitrogen-doped $TiO_2$ sputtered films intended for electrophotocatalytic applications under solar light. Journal of Applied Physics, 116 (2014), pp. 153510.

[44] E. Albiter, M. A. Valenzuela, , S. Alfaro, , G. Valverde-Aguilar, F. M. Martínez-Pallares, . Photocatalytic deposition of Ag nanoparticles on TiO2: Metal precursor effect on the structural and photoactivity properties. *Journal of Saudi Chemical Society*, *19*(2015), pp. 563-573.

[45] R. Pandiyan, N. Delegan, A. Dirany, P. Drogui, M. A. El Khakani, Probing the electronic surface properties and bandgap narrowing of in situ N, W, and (W, N) doped magnetron-sputtered $TiO_2$ films intended for electro-photocatalytic applications. The Journal of Physical Chemistry C, 120 (2016), pp. 631-638.

[46] Y. Gim, M. Seong, Y. W. Choi, J. Choi, $RuO_2$-doping into high-aspect-ratio anodic $TiO_2$ nanotubes by electrochemical potential shock for water oxidation. Electrochemistry Communications, 52 (2015), pp. 37-40.

[47] S. Rtimi, O. Baghriche, R. Sanjines, C. Pulgarin, M. Bensimon, J. Kiwi, TiON and TiON-Ag sputtered surfaces leading to bacterial inactivation under indoor actinic light. Journal of Photochemistry and Photobiology A: Chemistry, 256 (2013), pp. 52-63.

[48] Y. K. Lee, C. H. Jung, J. Park, H. Seo, G. A. Somorjai, J. Y. Park, Surface plasmon-driven hot electron flow probed with metal-semiconductor nanodiodes. Nano letters, 11 (2011), pp. 4251-4255.

[49] A. Pearson, H. Zheng, K. Kalantar-Zadeh, S. K. Bhargava, V. Bansal, Decoration of $TiO_2$ nanotubes with metal nanoparticles using polyoxometalate as a UV-switchable reducing agent for enhanced visible and solar light photocatalysis. Langmuir, 28 (2012), pp. 14470-14475.

[50] K. Chen, X. Feng, R. Hu, Y. Li, K. Xie, Y. Li, H. Gu, Effect of Ag nanoparticle size on the photoelectrochemical properties of Ag decorated $TiO_2$ nanotube arrays. Journal of alloys and compounds, 554 (2013), pp. 72-79.

[51] L. Yu, X. Yang, Y. Ye, X. Peng, D. Wang, Silver nanoparticles decorated anatase $TiO_2$ nanotubes for removal of pentachlorophenol from water. Journal of colloid and interface science, 453 (2015), pp. 100-106.

[52] M. M. Momeni, Y. Ghayeb, S. Gheibee, Silver nanoparticles decorated titanium dioxide-tungsten trioxide nanotube films with enhanced visible light photo catalytic activity. Ceramics International, 43 (2017), pp. 564-570.

[53] S. Rtimi, O. Baghriche, C. Pulgarin, R. Sanjines, J. Kiwi, Design, testing and characterization of innovative TiN–$TiO_2$ surfaces inactivating bacteria under low intensity visible light. RSC advances, 2 (2012), pp. 8591-8595.

[54] A. A. Ashkarran, S. M. Aghigh, N. J. Farahani, Visible light photo-and bioactivity of Ag/$TiO_2$ nanocomposite with various silver contents. Current Applied Physics, 11 (2011), pp. 1048-1055.

[55] P. Peerakiatkhajohn, W. Onreabroy, C. Chawengkijwanich, S. Chiarakorn, Preparation of visible-light-responsive $TiO_2$ doped Ag thin film on PET plastic for BTEX treatment. Journal of Sustainable Energy & Environment, 2 (2011), pp. 121-125.

[56] J. García-Serrano, E. Gómez-Hernández, M. Ocampo-Fernández, U. Pal, Effect of Ag doping on the crystallization and phase transition of $TiO_2$ nanoparticles. Current Applied Physics, 9 (2009), pp. 1097-1105.

[57] C. C. Chang, J. Y. Chen, T. L. Hsu, C. K. Lin, C. C. Chan, Photocatalytic properties of porous $TiO_2$/Ag thin films. Thin Solid Films, 516 (2008), pp. 1743-1747.

[58] Y. Zhou, C. Y. Wang, H. J. Liu, Y. R. Zhu, Z. Y. Chen, Preparation and studies of Ag–$TiO_2$ hybrid nanoparticles of core-shell structure. Materials Science and Engineering: B, 67 (1999), pp. 95-98.

[59] W. Elfalleh, A. A. Assadi, A. Bouzaza, D. Wolbert, J. Kiwi, S. Rtimi, Innovative and stable $TiO_2$ supported catalytic surfaces removing aldehydes under UV-light irradiation. Journal of Photochemistry and Photobiology A: Chemistry, 343 (2017), pp. 96-102.

[60] S. Rtimi, O. Baghriche, C. Pulgarin, J. C. Lavanchy, J. Kiwi, Growth of $TiO_2$/Cu films by HiPIMS for accelerated bacterial loss of viability. Surface and Coatings Technology 232 (2013), pp. 804-813.

[61] M. I. Mejia, J. M. Marin, G. Restrepo, L. A. Rios, C. Pulgarin, J. Kiwi, Preparation, testing and performance of a $TiO_2$/polyester photocatalyst for the degradation of gaseous methanol. Applied Catalysis B: Environmental 94 (2010), pp. 166-172.

[62] S. Rtimi, S. Giannakis, R. Sanjines, C. Pulgarin, M. Bensimon, J. Kiwi, Insight on the photocatalytic bacterial inactivation by co-sputtered $TiO_2$–Cu in aerobic and anaerobic conditions. Applied Catalysis B: Environmental 182 (2016), pp. 277-285.

[63] S. Rtimi, Indoor light enhanced photocatalytic ultra-thin films on flexible non-heat resistant substrates reducing bacterial infection risks. Catalysts 7 (2017), p. 57.

[64] S. Rtimi, S. Konstantinidis, N. Britun, V. A. Nadtochenko, I. A.Khmel, J. Kiwi, New Evidence for Ag-Sputtered Materials Leading to Bacterial Inactivation by Surface-Contact without the Release of Ag-ions: End of a Long Controversy? ACS Applied Materials & Interfaces 12 (2020) pp. 4998-5007.

[65] I. Fratoddi, Hydrophobic and hydrophilic Au and Ag nanoparticles. Breakthroughs and perspectives. Nanomaterials, 8 (2018), p. 11.

[66] T. Yuranova, A. G. Rincon, A. Bozzi, S. Parra, C. Pulgarin, P. Albers, J. Kiwi, Antibacterial textiles prepared by RF-plasma and vacuum-UV mediated deposition of silver. Journal of Photochemistry and Photobiology A: Chemistry, 161 (2003), pp. 27-34.

[67] T. Yuranova, A. Rincon, C. Pulgarin, D. Laub, X. Xanthopoulos, H-J. Mathieu, J. Kiwi, Performance and characterization of Ag-cotton and Ag/$TiO_2$ loaded textiles during the abatement of E. coli' J. Photochem. Photobiol A, 81 (2006), pp. 363-369.

[68] P. J. Kelly, H. Li, P. S. Benson, K. A. Whitehead, J. Verran, R. D. Arnell, I. Iordanova, Comparison of the tribological and antimicrobial properties of CrN/Ag, ZrN/Ag, TiN/Ag, and TiN/Cu nanocomposite coatings. Surface and Coatings Technology, 205 (2010), pp. 1606-1610.

[69] S. Rtimi, S. Konstantinidis, N. Britun, M. Bensimon, I. Khmel, V. Nadtochenko, Extracellular bacterial inactivation proceeding without Cu-ion release: Drastic effects of the applied plasma energy on the performance of the Cu-polyester (PES) samples. Applied Catalysis B: Environmental, 239 (2018), 245-253.

[70] W. L. Butler and D. W. Hopkins, Higher derivative analysis of complex absorption spectra. Photochem. and Photobiol. 12 (1970), pp. 439-450.

[71] I.M. Arabatzis, T. Stergiopoulos, M.C. Bernard, D. Labou, S.G. Neophytides, P. Falaras, Silver-modified titanium dioxide thin films for efficient photodegradation of methyl orange, Applied Catalysis B: Environment 42 (2003) 187-201.

[72] S. Sun, J. Bao, C. Gao, J. Ding, Photocatalytic degradation of gaseous o-xylene over M-$TiO_2$ (M= Ag, Fe, Cu, Co) in different humidity levels under visible-light irradiation: Activity and kinetic study. Rare Metals, 30 (2011), pp. 147-152.

[73] V. Vaiano, M. Matarangolo, J.J. Murcia, H. Rojas, J.A. Navío, M.C. Hidalgo, Enhanced photocatalytic removal of phenol from aqueous solutions using ZnO modified with Ag, Applied Catalysis B: Environmental 225 (2018) 197-206.

[74] K. Awazu, M. Fujimaki, C. Rockstuhl and J. Tominaga, A plasmonic photocatalyst consisting of silver nanoparticles embedded in titanium dioxide, J. Am.Chem. Soc. 130 (2008) 1676-1680.

[75] Rudolph A. Marcus, Nobel Lecture: Electron Transfer Reactions in Chemistry: Theory and Experiment, December 8, 1992.

[76] V. A. Nadtochenko, O. M. Sarkisov, V. V. Nikandrov, P. A. Chubukov, N. N. Denisov, Inactivation of Pathogenic Microorganisms in the Photocatalytic Process on Nanosized TiO2 Crystals, Russian Journal of Physical Chemistry B 2 (2008) 105–114.

[77] S. Rtimi and J. Kiwi, Update on Interfacial Charge Transfer (IFTC) Processes on Films Inactivating Viruses/Bacteria under Visible Light: Mechanistic Considerations and Critical Issues, Catalysts 11 (2021) 201.

[78] V. Nadtochenko and J. Kiwi, Photoinduced mineralization of xylidine by the Fenton reagent. 2. Implications of the precursors formed in the dark. Environmental Science & Technology 32 (1998) 3282-3285.

**Graphical abstract**

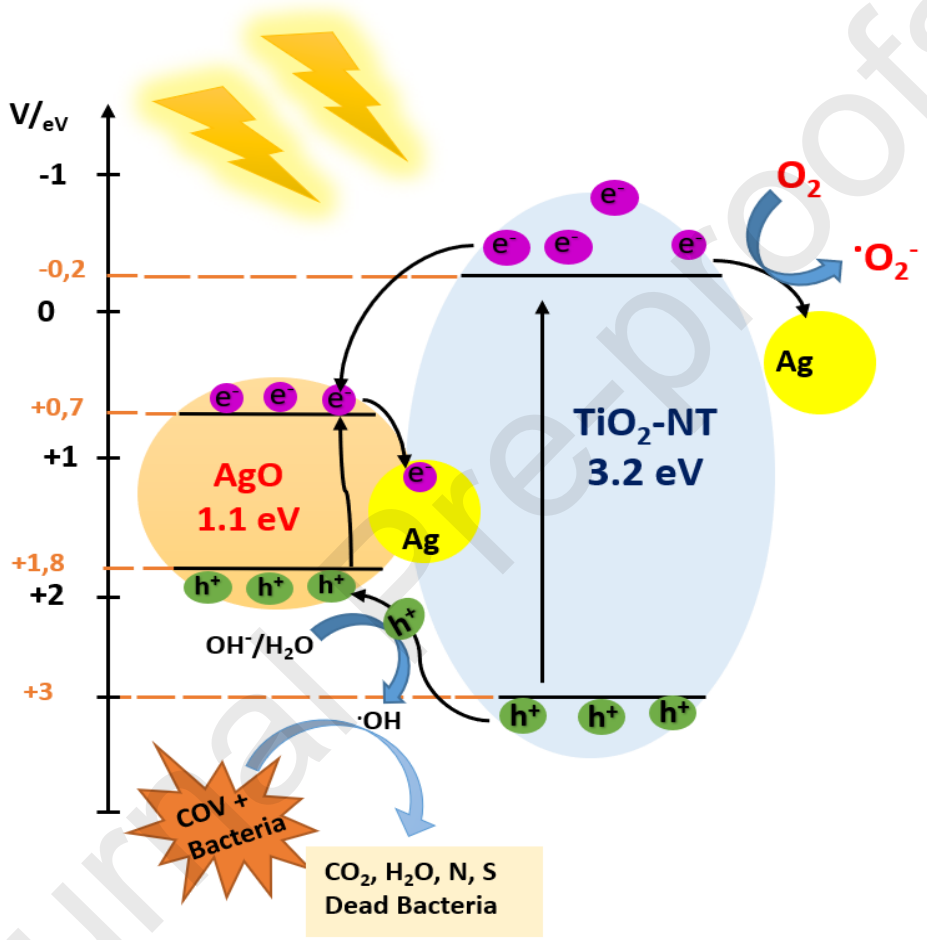


[79]

**Highlights**

- Indoor/outdoor air pollution and bacteria were degraded on sputtered $Ag_xO/Ag/TiO_2$ on textile.
- Photocatalytic kinetics are carried out in the dark and under visible light.
- Ag/AgxO nanoparticles show a significant effect on the activity of $TiO_2$.
- A possible mechanism of photocatalytic processes is suggested.

[80]